Reservoir crowding in a resource-constrained exclusion process with a dynamic defect

Bipasha Pal and Arvind Kumar Gupta*
Department of Mathematics, Indian Institute of Technology Ropar, Rupnagar 140001, Punjab, India

(Received 3 August 2022; accepted 3 October 2022; published 21 October 2022)

To understand the complicated transport processes that occur in biological and physical systems, we investigate a constrained totally asymmetric simple exclusion process with a stochastic defect particle. The defect particle might randomly emerge or vanish, resulting in a dynamic defect, and slows down the flow of moving particles when attached to the lattice. Using a mean-field technique, we examine the steady-state characteristics and boundary-layer analysis is provided to comprehend the properties of finite system. In a simplification, our theoretical method unifies three different parameter used to define the defect dynamics into one parameter termed the obstruction factor. It is found that the defect kinetics lead to emergence of phases where the current is defect restricted. The system shows nine phases overall, including bulk-induced and boundary-induced shock phases, with the phase schema showing no more than eight phases depending on the dynamics. We found that variation of obstruction does not lead to qualitative transition in the system, whereas the change in constraint on total particles affect the system qualitatively. All the theoretical outcomes have been validated using extensive Monte Carlo simulations.

DOI: 10.1103/PhysRevE.106.044130

I. INTRODUCTION

In recent years, there has been a surge of interest across the investigation of complicated nonequilbrium events in a wide range of topics spanning from physics to biology [1–7]. In contrast to the study of thermodynamically balanced systems, no general theoretical framework for determining the attributes of aforementioned systems exists. As a result, paradigmatic models play an important role in understanding the physics of nonequilibrium systems. Totally Asymmetric Simple Exclusion Process (TASEP) is one such model that provides a framework for understanding properties in these systems [3,8–12]. Furthermore, it has been frequently utilized to investigate nonequilibrium features in a wide range of phenomena, including vehicular traffic [13,14], intracellular transport [3,15,16], transcription and translation [15,17–21], etc. In the simplest variant of the TASEP, particles hop stochastically in one direction on a lattice with unit rate and are prohibited to fill the positions that are preoccupied by another particle. The nonequilbrium steady state of the TASEP has been precisely solved with a matrix formalism or similar approaches such as a Bethe ansatz under open boundary conditions [11,22,23]. It has been found that the system exhibits three distinct phases namely low density (L), high density (H), and maximal current (M). The L phase occurs when the particle flux is restricted by particle entrance, the H phase when particle exit restricts the flow, and the M phase when the flow is limited by the system's interior regardless of the boundary rates.

This primary model has been generalized with various dynamics, multiple species of particles, or a spatial dependency of the rates for many of the applications [24–29]. The majority of the literature uses open TASEPs to examine the collective behavior of particles on a lattice supplied with an unlimited reservoir, thus maintaining consistent entrance and exit rates regardless of reservoir occupancy, which may not be realistic in a majority of cases. In actuality, resources are limited in physical and biological systems, which has nontrivial impact on the dynamics owing to competition for resources. In recent years, a variation of the TASEP model has developed where the total number of particles in the system is preserved and depicts the global constraint on the resources in almost all physical and biological systems [30–35]. As a result of this, a new phase known as shock phase (S) emerges admitting a localized domain wall which appears as a shock in the density profile. All of these studies have looked at TASEP models in confined environments with a primary focus on how limited resources affect the pace at which particles enter the lattice. The restricted capacity of the reservoir, however, can also have an impact on the particle exit rates. For example, when a vehicle intends to leave the road and enter into a parking garage, the impediments caused by cars in a packed garage lower the exit rate from the road. Recent research has focused on a TASEP version that may accurately imitate these situations by accounting for the impact of reservoir occupancy on departure and entrance rates [36,37]. This characteristic is known as reservoir crowding which has been proposed as a way by which the particles escape the reservoir's overcrowding.

Another factor that is important to many applications and is frequent in everyday life is the existence of imperfections that delay or temporarily block particle flow. Examples include traffic regulation and halted cars in vehicular traffic [1], nucleic acid binding proteins in transcription and translation [38,39], etc. These defects such as blockages, roadblock particles, etc., can be static or dynamic, and they have a significant

*akgupta@iitrpr.ac.in

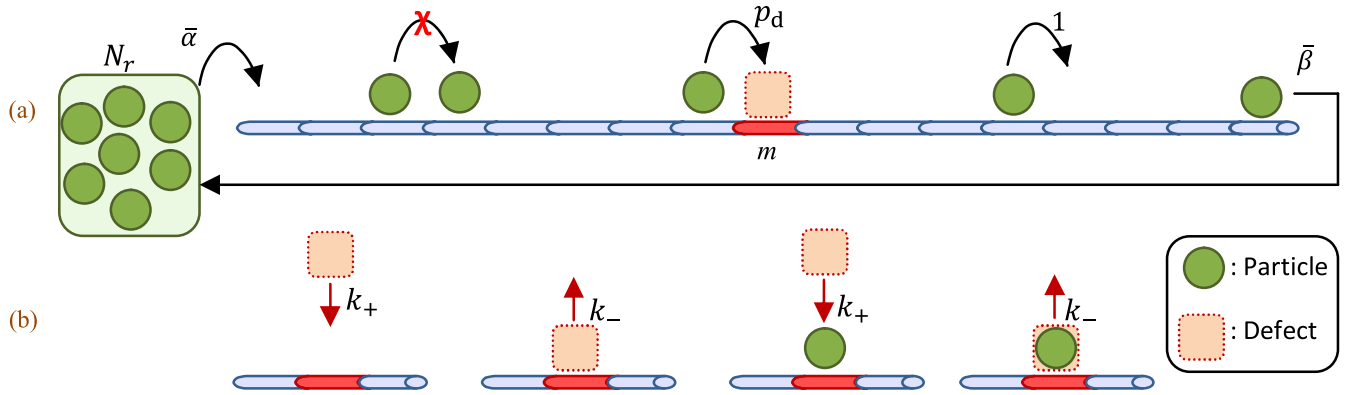

FIG. 1. (a) Schematic representation of the TASEP model featuring reservoir crowding with a dynamic defect at special site m. Circles denote the particles, whereas square represents the defect at mth site. (b) Association and dissociation rates of defect at that mth site that remain independent of presence or absence of particle.

influence on particle dynamics. When the obstacles are static, the special sites are given hopping rates permanently which are distinct from ordinary sites and have received extensive research [27,40–42]. On the other hand, defects or dynamic obstacles may appear and disappear stochastically. Dynamic obstacles cause the particle mobility to slow down or stop; otherwise, when unobstructed, the particle proceeds at its typical hopping rate. Such unconstrained disordered systems have been explored under the TASEP framework, where the defect may emerge or disappear at random on particular sites, causing a different hopping rate from other sites [43–45]. A model with periodic boundaries having one-site dynamical defect has been studied where the site can stochastically achieve the state of being closed or open [46]. When open, it allows the flow of particles and on closing, it blocks particle movement. Several other studies with open boundaries contain a defect particle which will generally limit the maximum feasible flow to a value less than the maximal flux in the absence of defects [43–45]. As a result, the M phase of the conventional TASEP is replaced by a defect-restricted phase, in which the flux is no longer governed by the boundary rates, but by the dynamics at the defect.

In contrast to the lattice that represents microtubules or roads and is considered to be homogeneous throughout, the actual pathway may depict imperfections. In biological transport, research reveal that the enzymes can alter tubulin units *in vivo* [47]. Also, the microtubule-associated proteins can bind to and unbind from the microtubule [38,39,48]. Thus, the cell may regulate the motor transport characteristics via inhomogeneities or microtubule decoration elements. These may disrupt the traffic of molecular motors and to fully describe the such processes, and all these factors must be taken into account. Similarly, in vehicular transport, a traffic light may interrupt the movement of vehicles. In such systems, the available resources are limited. Motivated by these, we investigate a generic roadblock model with a defect that stochastically unbinds-rebinds from a single site and, when bound, stops or slows down the passage of actively moving particles. We use a mean-field approximation to conceptually approach the system in order to study the dynamics of the suggested model. The structure of our paper is as follows. We describe the model and its dynamic rules in Sec. II. In Sec. III, we lay out our methodology and offer the mathematical treatment of our model. This is followed by an examination of the kinetics of our suggested model. Using our theoretical framework, we examine potential stationary phases in Sec. IV. The technical aspects of the Monte Carlo simulation are then explained and the results are discussed in Sec. V, followed by a summary of our findings in Sec. VI.

II. MODEL DEFINITION

We consider a minimal model for nonequilibrium transport processes that depicts the essential components such as microtubules, roadways, etc., as a lattice and entities traveling along these channels as particles. The one-dimensional lattice consists of $2\times L$ sites and both of its ends are connected to a single reservoir having a finite number of identical particles denoted by N_r, as depicted in Fig. 1. At any time, the total number of particles in the system, N_{tot}, remains constant, effectively reflecting the limited resources in biological and physical systems. Particles are allowed to enter the lattice from the first site, provided it is empty, with a modified entry rate regulated according to the particles available in the reservoir. This rate, indicated by $\bar{\alpha}$ is given by

$$\bar{\alpha} = \alpha f(N_r), \tag{1}$$

where α is the inherent entry rate of the particles in the absence of any constraint on the available resources. The particles can leave the lattice from the last site with a modified exit rate, $\bar{\beta}$, which also depends on the occupancy of the reservoir and is expressed as

$$\bar{\beta} = \beta g(N_r). \tag{2}$$

In the above equation, β signifies the inherent exit rate in the absence of a crowding characteristic. All particles move in the same direction along the lattice, obeying the hardcore exclusion principle, as shown in Fig. 1.

Due to the feature of reservoir crowding in our model, we are investigating a situation in which a higher particle content in the reservoir enhances particle inflow into the lattice while lowering particle outflow from the lattice to the reservoir. Therefore, it is plausible to assume $f(N_r)$ and $g(N_r)$ to be monotonically increasing and decreasing functions of N_r,

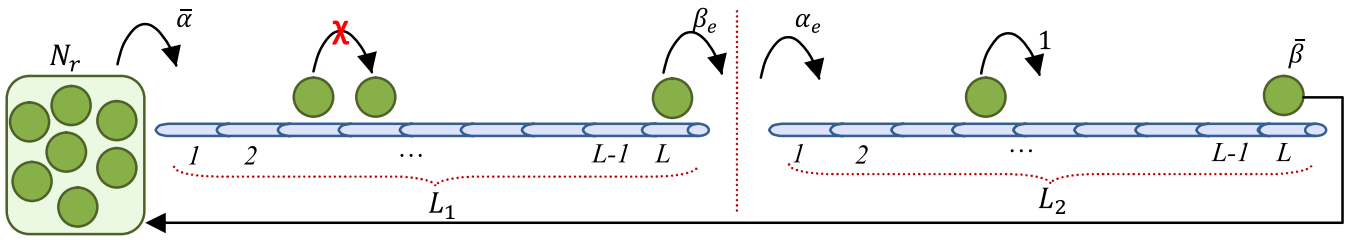

FIG. 2. Decomposition of the inhomogeneous system into two coupled homogeneous sublattices: L_1 and L_2.

respectively. As the simplest choice, these functions are defined as

$$f(N_r) = N_r/N_{\text{tot}}, \quad g(N_r) = 1 - N_r/N_{\text{tot}}, \tag{3}$$

and are bounded between 0 and 1 [36]. As a result, the modified rates are confined within 0 and the inherent rates. Intending to investigate the influence of the total number of particles on the system dynamics, we designate a parameter—filling factor—defined as $\mu = \frac{N_{\text{tot}}}{2L}$ [30,36], which depicts the population of the system relative to the lattice size.

It is also assumed that another form of particle, known as a dynamic defect, can attach to a particular site m located away from both ends of the lattice. We fix that site to be $m = L + 1$ for our analysis. The defect binds to the lattice at a rate k_+ if it is free from the defect and unbinds at a rate k_- if it is not irrespective of the site's occupancy by a particle; see Fig. 1(b). Although the existence of particles has no effect on the defect's transition rates at site $i = m$, it does affect the particle's hopping rates from sites $m - 1$ to m. If the defect is present, then the particle leaps at a decreased rate of $p_d \leqslant 1$ from site $m - 1$ to m; else, it hops with the unit rate. The defect's impact is highest if $p_d = 0$, but when $p_d = 1$, the particles are completely unaware of the defect's presence. If both the particle and the defect are present at site m, then the particle's hopping rate to site $m + 1$ stays 1. It must be noted that the dynamic defect is different than static counterpart; setting $p_d = 0$ in present model does not mean that particle flux is zero which happens in case of static defect [27].

Due to the presence of a dynamic defect at site m, the transition rates of the particles are locally affected introducing an inhomogeneity in the system. For analytical amenability, we partition the lattice into two homogeneous sublattices: L_1 and L_2 as illustrated in Fig. 2. Each sublattice has L sites which are labeled as $i = 1, 2, \ldots, L$. In our theoretical paradigm, β_e represents the particle's effective exit rate from L_1 and α_e represents the particle's effective entrance rate into L_2. From here onward, we refer to α_e, β_e, $\bar{\alpha}$, and $\bar{\beta}$ collectively as altered rates. These rates have to be evaluated, and to achieve this we note that the sublattices thus obtained are coupled as follows. First, due to the reservoir crowding feature, the rates $\bar{\alpha}$ and $\bar{\beta}$ are linked. Second, owing to the continuity of current, equal particle currents must flow through both sublattices in the steady-state regime. Taking these into account, the altered entry and exit rates for both the sublattices have to be accessed to describe the dynamics of the decomposed system. In the next section, we delineate the mathematical treatment of the proposed model.

III. MATHEMATICAL ANALYSIS

We define $\tau_{i,k}$ as the occupancy number of particles at the ith site of the sublattice L_k where $k \in \{1, 2\}$. Owing to hard-core exclusion, $\tau_{i,k}$ can only accept binary values, 0 and 1 if the ith site of the sublattice L_k is empty or occupied by a particle, respectively. Furthermore, we designate the defect's occupancy number by η, which takes the value 1 in presence of defect and 0 when not filled by a defect. The master equations for the evolution of bulk particle density of both sublattices are provided by

$$\frac{d\langle\tau_{i,k}\rangle}{dt} = J_k^{i-1,i} - J_k^{i,i+1}, \quad 1 < i < L, \tag{4}$$

where $\langle \ldots \rangle$ denote the statistical average and the term $J_k^{i,i+1}$ is the current passing from site i to $i + 1$ in sublattice L_k defined as

$$J_k^{i,i+1} = \langle\tau_{i,k}(1 - \tau_{i+1,k})\rangle. \tag{5}$$

At the boundaries of sublattice L_1, the densities evolve according to

$$\begin{aligned} \frac{d\langle\tau_{1,1}\rangle}{dt} &= \bar{\alpha}\langle 1 - \tau_{1,1}\rangle - J_1^{1,2}, \\ \frac{d\langle\tau_{L,1}\rangle}{dt} &= J_1^{L-1,L} - \beta_e\langle\tau_{L,1}\rangle, \end{aligned} \tag{6}$$

whereas the evolution of density in the boundaries of the sublattice L_2 is governed by

$$\begin{aligned} \frac{d\langle\tau_{1,2}\rangle}{dt} &= \alpha_e\langle 1 - \tau_{1,2}\rangle - J_2^{1,2}, \\ \frac{d\langle\tau_{L,2}\rangle}{dt} &= J_2^{L-1,L} - \bar{\beta}\langle\tau_{L,2}\rangle. \end{aligned} \tag{7}$$

Solving Eqs. (4)–(7) is intractable in the present form due to the presence of both one-point and two-point correlators. Therefore, the mean-field approximation is used, with all correlations discarded and the correlators calculated as follows:

$$\begin{aligned} \langle\tau_{i,k}\,\tau_{i',k'}\rangle &= \langle\tau_{i,k}\rangle\langle\tau_{i',k'}\rangle, \\ \langle\eta\,\tau_{i,k}\rangle &= \langle\eta\rangle\langle\tau_{i,k}\rangle, \end{aligned} \tag{8}$$

where $i, i' \in \{1, 2, \ldots, L\}$ and $k, k' \in \{1, 2\}$. Using the mean-field approximation and coarse-graining the discrete lattice with the lattice constant $\epsilon = 1/L$ to a continuum limit followed by time rescaling as $t' = t/L$, we obtain the subsequent continuum equation for the bulk of sublattices,

$$\frac{\partial\rho_k}{\partial t} = \frac{\epsilon}{2}\frac{\partial^2\rho_k}{\partial x^2} - \frac{\partial J_k}{\partial x}. \tag{9}$$

Here $x = i/L$, $0 \leqslant x \leqslant 1$ is the rescaled position variable, and ρ_k produces the average particle density of the sublattice L_k. Moreover, the current in the sublattice L_k is expressed as $J_k = \rho_k(1-\rho_k)$. In steady state, Eq. (9) supplemented with boundary conditions is expressed as follows:

$$\frac{\partial J_k}{\partial x} - \frac{\epsilon}{2}\frac{\partial^2 \rho_k}{\partial x^2} = 0, \tag{10}$$

$$\rho_1(0) = \bar{\alpha}, \quad \rho_1(1) = 1-\beta_e, \tag{11}$$

$$\rho_2(0) = \alpha_e, \quad \rho_2(1) = 1-\bar{\beta}. \tag{12}$$

In the limit $\epsilon \to 0$, the differential equation in Eq. (10) simplifies to $\frac{\partial J_k}{\partial x} = 0$, implying that the current through each sublattice is constant.

Due to the presence of the second-order derivative term with very small coefficient ϵ, Eq. (10) is a singular equation. The singularity derives from the fact that in the limit $\epsilon \to 0$, the aforementioned equation simplifies to a first-order equation that cannot satisfy two boundary conditions in general. Solved solutions to such singular equations are known to feature boundary layers whose width is substantially dependent on the coefficient ϵ.

With the division of the proposed system into two homogeneous sublattices, each subsystem can now be evaluated as an open TASEP supplemented with their respective altered entry and exit rates. Our goal is to explicitly evaluate the following rates: $\bar{\alpha}$, $\bar{\beta}$, α_e, and β_e. To achieve this, we intend to utilize the coupling of the sublattices owing to the conservation of current across the defect site and regulation of entry-exit rates due to constrained resources. We begin with analyzing the kinetics of the dynamic defect whose temporal evolution equation at site m is expressed as

$$\frac{d\langle\eta\rangle}{dt} = \langle 1-\eta\rangle k_+ - \langle\eta\rangle k_-. \tag{13}$$

In the above equation, $\langle\eta\rangle \equiv \rho^*$ yields the defect density, which attains the following value in steady state:

$$\rho^* = \frac{k_+}{k_+ + k_-}. \tag{14}$$

When $k_+ = 0$, the defect can never attach to the lattice at any time and hence its density, calculated by Eq. (14), takes the value 0. The proposed model simplifies to the open TASEP with reservoir crowding [36], which is homogeneous throughout the lattice. However, the defect dynamics disrupt the homogeneity of our system, and therefore the lattice is selectively broken upstream of the special site m to obtain two coupled homogeneous subsystems.

Due to the conservation of current throughout the lattice, the current in both subsystems must be equal, that is, $J_1 = J_2$. The expression for current in the bulk yields $\rho_1(1-\rho_1) = \rho_2(1-\rho_2)$, which provides us with two options:

$$\rho_1 = \rho_2 \text{ or } \rho_1 = 1-\rho_2. \tag{15}$$

Furthermore, the current flowing from the site $m-1$ to m, denoted as J_{link}, connects the two sublattices and is given by

$$J_{\text{link}} = \rho^* J_d + (1-\rho^*)\hat{J}_d. \tag{16}$$

In the above equation, J_d and $\hat{J}_d$ indicate the current from the site $m-1$ to m in the presence and absence of defect kinetics, respectively, which are expressed as

$$J_d = p_d \hat{J}_d \quad \text{and} \quad \hat{J}_d = \rho_1(1)[1-\rho_2(0)]. \tag{17}$$

Also, the current exiting from L_1, $J_{\text{exit},1}$ and the current entering L_2, $J_{\text{enter},2}$ are represented as follows:

$$J_{\text{exit},1} = \beta_e \rho_1(1), \quad J_{\text{enter},2} = \alpha_e[1-\rho_2(0)]. \tag{18}$$

Invoking the continuity of current implies $J_{\text{exit},1} = J_{\text{link}} = J_{\text{enter},2}$, which yields the following expression for α_e and β_e:

$$\begin{aligned} \alpha_e &= \rho_1(1)[1-\rho^*(1-p_d)], \\ \beta_e &= [1-\rho_2(0)][1-\rho^*(1-p_d)]. \end{aligned} \tag{19}$$

The obstruction provided by defect is directly proportional to its density and inversely proportional to the slowdown rate. Thus, we define $z = \rho^*(1-p_d)$ to be the obstruction factor which quantifies the hindrance provided to particle flow. We use this parameter hereafter because it is beneficial in two ways. It reduces the parameter space and simplifies the ensuing expressions.

To determine the modified entry rates $\bar{\alpha}$ and $\bar{\beta}$, we utilize the particle number conservation (PNC) which states that $N_r + N_L = N_{\text{tot}}$, and N_L denotes the number of particles on the lattice. This relation in its continuum form gives

$$\frac{1}{2}\int_0^1 \rho_1 dx + \frac{1}{2}\int_0^1 \rho_2 dx + r = \mu, \tag{20}$$

where $r = \frac{N_r}{2L}$ signifies the quotient of the reservoir. On plugging the values of ρ_1 and ρ_2, r is obtained explicitly. In terms of quotient of reservoir, the modified rates can be rewritten as

$$\bar{\alpha} = \alpha r/\mu \quad \text{and} \quad \bar{\beta} = \beta(1-r/\mu). \tag{21}$$

The expressions for the altered rates will be provided explicitly in the upcoming sections. In the next section, we provide the theoretical approach to obtain the density profiles which will be later used to characterize the system.

A. Boundary-layer analysis

In real situations, the system size L is finite, implying that ϵ may not approach 0 and thus, the boundary layer cannot be neglected. Therefore, we utilize the boundary-layer analysis to fully describe the density profiles which mainly involves two stages [28,29]. At the first stage, the slowly varying solution, referred to as the outer solution, is obtained, which describes the bulk of the density profile. The rapidly fluctuating component of the density profile solution, known as the inner solution, which appears in a limited section of the lattice, is then calculated. Finally, the asymptotic matching of the outer and inner solutions yields a uniformly valid solution for the density profile. Following this technique, we recall the solution for a possible collection of boundary conditions.

B. Outer solution

The solutions for the bulk of the density profiles, ρ_k, are derived by setting $\epsilon = 0$ in Eq. (10). This results in the following

expression for the outer solution $\rho_{\text{out},k}$:

$$\rho^{\pm}_{\text{out},k} = \frac{1}{2} \pm \frac{1}{2}\sqrt{1+4c_k}, \tag{22}$$

where c_k is the constant of integration and $k \in \{1, 2\}$. The value of c_k can be calculated using the boundary condition that the outer solution for sublattice L_k meets. For instance, if the solution for sublattice L_1 satisfies the boundary condition $x = 0$, i.e., $\rho^{\pm}_{\text{out},1}(0) = \bar{\alpha}$, then $c_1 = \bar{\alpha}(\bar{\alpha} - 1)$. If, on the other hand, the outer solution matches the boundary condition at $x = 1$, then $c_1 = \beta_e(\beta_e - 1)$. Clearly, from Eq. (22), in any of these scenarios, the outer solutions are always constant.

C. Inner solution

In order to obtain the boundary-layer part, the second-order term in Eq. (10) is crucial. To find the inner solution $\rho_{\text{in},k}$, Eq. (10) is expressed in terms of $\tilde{x} = (x - x_0)/\epsilon$ (where x_0 denotes the position of boundary layer) and then consider $\epsilon \to 0$. The second-order differential equation with respect to $\tilde{x}$ is given by

$$\frac{1}{2}\frac{d^2\rho_{\text{in},k}}{d\tilde{x}^2} + (2\rho_{\text{in},k} - 1)\frac{d\rho_{\text{in},k}}{d\tilde{x}} = 0, \tag{23}$$

which, on integration, gives

$$\frac{1}{2}\frac{d\rho_{\text{in},k}}{d\tilde{x}} + \rho^2_{\text{in},k} - \rho_{\text{in},k} = b_k, \tag{24}$$

whereb_k denotes the integration constant. Due to the fact that the boundary-layer saturates to the outer solution in the suitable limit of $\tilde{x}$, $b_k = \rho^2_{b,k} - \rho_{b,k}$, where $\rho_{b,k}$ is the bulk density to which the boundary-layer solution saturates. The possible solutions of the Eq. (24) are given as

$$\rho_{\text{in},k} = \frac{1}{2} + \frac{d_{1,k}}{2}\coth[c_1(\tilde{x} + d_{2,k})], \tag{25}$$

$$\rho_{\text{in},k} = \frac{1}{2} + \frac{d_{1,k}}{2}\tanh[c_1(\tilde{x} + d_{2,k})], \tag{26}$$

where $d_{1,k}$ and $d_{2,k}$ are the integration constants whose values are obtained through the boundary conditions for sublattice L_k which the boundary-layers solution must satisfy.

D. General form of solutions

Here we refer to the general solutions of various phases corresponding to generic boundary conditions for the sublattice L_1, which may be extended to the other sublattice in a similar manner.

1. Low-density phase

In this case, the outer solution satisfies the boundary condition at $x = 0$ and the boundary layer satisfies the condition at $x = 1$. In such a phase, $\bar{\alpha} < 1/2$ and $\beta_e > \bar{\alpha}$. The outer solution $\rho^{-}_{\text{out},1}$ with $c_1 = \bar{\alpha}(\bar{\alpha} - 1)$ is described by Eq. (22) and the boundary layer must saturate to outer solution as $x \to 1^-$. If $1 - \beta_e > \bar{\alpha}$, then the boundary layer must have positive slope to satisfy the boundary condition and is described by a tanh-type solution [Eq. (26)], whereas for $1 - \beta_e < \bar{\alpha}$, the negative slope of the boundary-layer solution prompts the use of coth-type solution [Eq. (25)]. The constants are obtained by utilizing the boundary matching at $x_0 = 0, -\infty$, and ∞.

2. Shock phase

When this situation arises, the boundary layer deconfines from the $x = 1$ and enters the bulk, which appears as a stationary shock. The position of this shock is determined using the particle number conservation, which we discuss in detail in Appendix B. Then the outer solution has two parts, one with $\rho^{-}_{\text{out},1} < 1/2$ satisfying the left boundary condition and the another one with $\rho^{+}_{\text{out},1} > 1/2$ satisfying the right boundary condition, with these two parts being separated by a boundary layer of tanh-type [Eq. (26)].

3. High-density phase

The boundary layer in high-density phase appears near $x = 0$. When $\bar{\alpha} > 1 - \beta_e$, the boundary layer has a positive slope to meet the boundary condition and is characterized by coth-type solution [Eq. (25)], but when $\bar{\alpha} < 1 - \beta_e$, the boundary later solution has a negative slope which calls for the usage of tanh-type solution [Eq. (26)]. By using the boundary matching at $x_0 = 0, -\infty$, and ∞, the constants are found.

The above discussion provides the complete solution to the density profile of sublattice L_1, which can be extended similarly to L_2 provided the altered rates are known. Alternatively, the density profiles can be obtained by utilizing numerical schemes, which is provided in Appendix A. In the next section we delineate the methodology to obtain these rates, which will aid in completely characterizing the system properties.

IV. STATIONARY PHASES AND THEIR PROPERTIES

In this part, we discuss the possible phases and provide explicit expressions for the altered entrance and exit rates, which are essential to fully define the system's stationary features. We briefly recall the stationary properties of the homogeneous open TASEP that has been well studied using a mean-field approach [49–51]. It was found that the system can be in one of the following phases depending on the entry and exit rates, which are referred to as entry-dominated low density (L), exit-dominated high density (H), and bulk-dominated maximal current (M). When the entry rate is lower than exit rate while being less than 0.5, the system displays low density. For the scenario where the entry rate exceeds the exit rate and the latter is less than 0.5, the system is in a high-density phase. In the case of entry and exit rates both greater than 0.5, the maximal current phase occurs. The transition from both the L and H phases to the M phase is of second order with respect to the density. However, the phase transition from L to H is of first order, and in this line (when entry equals the exit rate), a low-high density coexistence phase appears which admits a delocalized shock wandering throughout the lattice. It is seen that as soon as a constraint is placed on the number of particles in the system, the shock is pinned in a position [30,31,34,35]. This shock was found to be boundary induced. Moreover, the region of low-high density coexistence phase does not remain limited to a line and is referred to as the shock (S) phase.

Now we provide the notation for a probable phase as A/B for clarity, where A and B are the phases indicated by sublattices L_1 and L_2, respectively. As each sublattice can have one of the four phases (L, H, M, and S), our system can have up to $4^2 = 16$ different phases. However, due to the current

TABLE I. Summary of existence conditions as well as the altered rates that are obtained theoretically. Here L, H, S, S*, and M indicate the low-density phase, high-density phase, boundary-induced shock phase, bulk-induced shock phase, and maximal current phase, respectively. L/H phase appears in the transition line between the L/S and S/H phases.

Phase	Existence regions	$\bar{\alpha}$	$\bar{\beta}$	α_e	β_e
L/L	$\bar{\alpha} < \beta_e, \bar{\alpha} < 1/2, \alpha_e < \bar{\beta}, \alpha_e < 1/2$	$\frac{\alpha\mu}{\alpha+\mu}$	$\frac{\alpha\beta}{\alpha+\mu}$	$\frac{\alpha\mu}{\alpha+\mu}$	$\left(1-\frac{\alpha\mu}{\alpha+\mu}\right)(1-z)$
H/H	$\bar{\alpha} > \beta_e, \beta_e < 1/2, \alpha_e > \bar{\beta}, \bar{\beta} < 1/2$	$\frac{\alpha(-1+\beta+\mu)}{\beta+\mu}$	$\frac{\beta}{\beta+\mu}$	$\frac{\mu(1-z)}{\beta+\mu}$	$\frac{\beta}{\beta+\mu}$
L/S	$\bar{\alpha} < \beta_e, \bar{\alpha} < 1/2, \alpha_e = \bar{\beta} < 1/2$	$\frac{\alpha\beta}{\alpha+\beta}$	$\frac{\alpha\beta}{\alpha+\beta}$	$\frac{\alpha\beta}{\alpha+\beta}$	$\left(1-\frac{\alpha\beta}{\alpha+\beta}\right)(1-z)$
S/H	$\bar{\alpha} = \beta_e < 1/2, \alpha_e > \bar{\beta}, \bar{\beta} < 1/2$	$\frac{\alpha\beta}{\alpha+\beta}$	$\frac{\alpha\beta}{\alpha+\beta}$	$\frac{\alpha\beta}{\alpha+\beta}$	$\left(1-\frac{\alpha\beta}{\alpha+\beta}\right)(1-z)$
H/L	$\bar{\alpha} > \beta_e, \beta_e < 1/2, \alpha_e < \bar{\beta}, \alpha_e < 1/2$	$\alpha\left(1-\frac{1}{2\mu}\right)$	$\frac{\beta}{2\mu}$	$\frac{1-z}{2-z}$	$\frac{1-z}{2-z}$
S*/L	$\bar{\alpha} = \beta_e < 1/2, \alpha_e < \bar{\beta}, \alpha_e < 1/2$	$\frac{1-z}{2-z}$	$\frac{\beta\left[(1-z)(\alpha-1)+\alpha\right]}{\alpha(2-z)}$	$\frac{1-z}{2-z}$	$\frac{1-z}{2-z}$
H/S*	$\bar{\alpha} > \beta_e, \beta_e < 1/2, \alpha_e = \bar{\beta} < 1/2$	$\frac{\alpha\left[(1-z)(\beta-1)+\beta\right]}{\beta(2-z)}$	$\frac{1-z}{2-z}$	$\frac{1-z}{2-z}$	$\frac{1-z}{2-z}$
M/M	$\bar{\alpha} > 1/2, \bar{\beta} > 1/2$	$\alpha\left(1-\frac{1}{2\mu}\right)$	$\frac{\beta}{2\mu}$	$\frac{1}{2}$	$\frac{1}{2}$

continuity requirement across both the sublattices, not all of them exist. Thus, the prospect of having the M phase in one sublattice and the L, H, or S phase in the other, accounting for six distinct phases, may be ruled out based on the physical argument that these phases support different particle currents. The circumstances of the existence of remaining possible phases need to be investigated theoretically.

The effective rates α_e and β_e, as well as the reservoir densities for all viable phases are to be determined, which will be utilized to obtain the existential conditions of the conceivable phases. In this direction, we proceed along the following steps. Assuming that the system is in one of the probable phases, we know their distinctive density profile. Employing this fact as well as the expression for current and its continuity, the altered rates are accessed in terms of reservoir quotient. Subsequently, particle number conservation is incorporated to obtain the reservoir quotient (except when at least one of sublattice is in the S phase whose methodology is detailed in Appendix B) which yields the altered densities. Having explicit values for these quantities, the conditions of existence of the phases can be verified. As a result, by contrasting the expected and actual phases, a self-consistency check is offered.

By utilizing the above outlined methodology, the existence conditions of the altered rates of the possible phases are mentioned in Table I and the detailed analysis are provided in Appendix B. It is found that the dynamics lead to a defect-restricted phase, namely H/L, which is reminiscent of the maximal current phase in the analogous model without the defects [36]. The current sustained in this phase corresponds to the maximum magnitude that the proposed model can exhibit with respect to the defect dynamics. Moreover, our theoretical analysis identifies two distinct types of shock phases: boundary induced and bulk induced. In order to distinguish between them, we will hereafter refer to the shock phase in a sublattice that is bulk induced as S* and its counterpart that is boundary induced as S. In the sections that follow, these are covered in detail. In addition to the H/L phase, the bulk-induced S*/L and H/S* phases also correspond to defect-restricted phase whose current is regulated by the defect dynamics irrespective of entry-exit rates.

In the next section, we examine the effects of various dynamics on the system properties.

V. RESULTS AND DISCUSSION

Our goal is to study the influence of finite resources in terms of μ as well as the impact of defect kinetics quantified by z on the system's stationary properties. In this direction, we use the analysis provided in previous sections to investigate the system behavior in the α-β plane. To validate our theoretical results, we perform Monte Carlo simulations with a system size of $L = 1000$. The computer simulations are run for 5×10^9 time steps, with the first 5% of the time steps scraped to assure occurrence of steady state. We quickly mention that the system has been tested for various other pair of functions as an alternate form for Eq. (3). The consistency of simulation data and analytical predictions for all the regimes is equally impressive, although we will not get into specifics here. Nevertheless, the functional form of f and g is likely to have a significant impact on the phase boundaries.

We now specify investigate the influence of several parameters in the dynamics of defect in the presence of constrained resources.

A. Effect of filling factor

In this study, filling factor μ represents the average number of particles available for each lattice site effectively representing how much filled the system is. We expect filling factor to significantly affect the stationary properties: scarcity of particles leads to a steady state with lower densities, whereas in presence of sufficient number of particles, the system may exhibit the steady state with higher densities depending on the entry and exit rates.

Figure 3 shows the stationary phase diagrams for various values of filling factors displaying the topological disparities while keeping the obstruction factor unchanged. Theoretically, one may determine the crucial points at which these

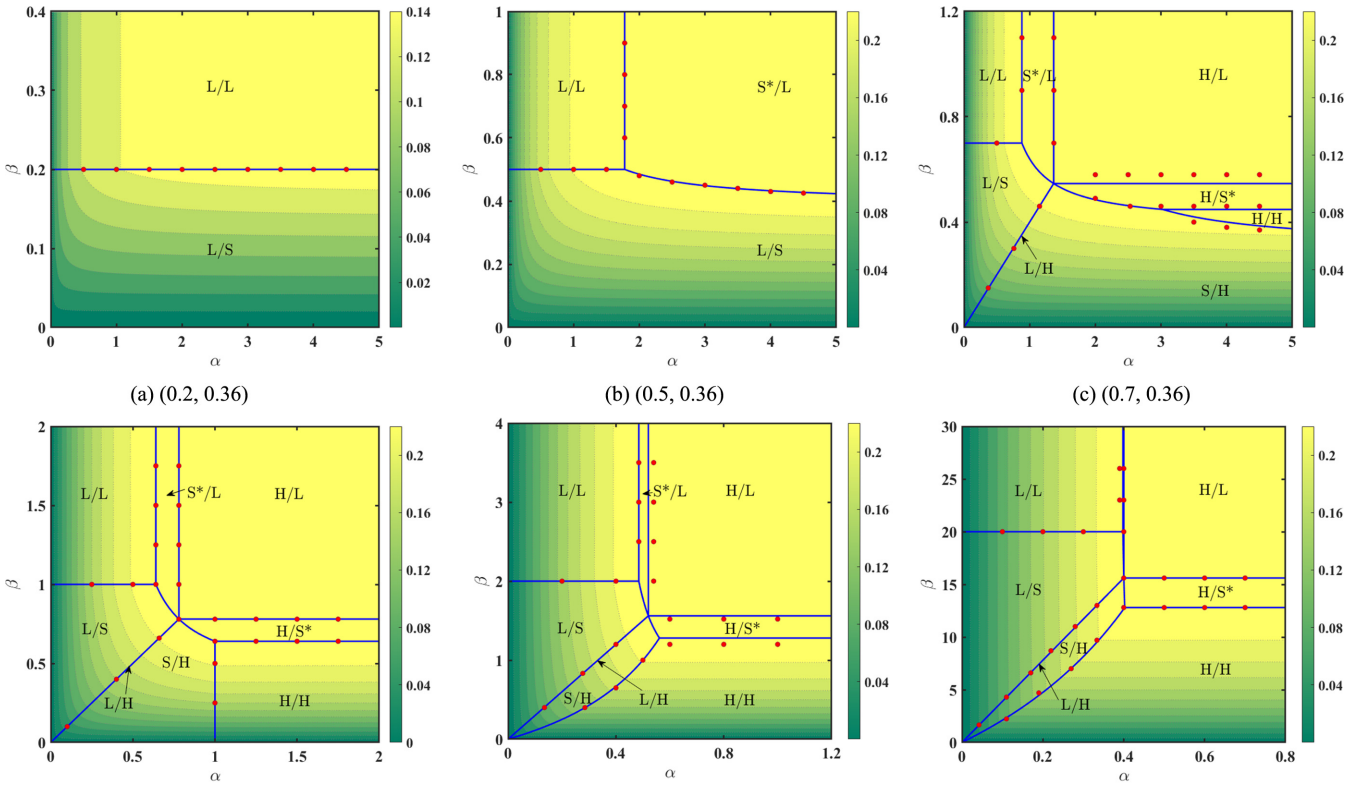

(a) (0.2, 0.36) (b) (0.5, 0.36) (c) (0.7, 0.36)

(d) (1, 0.36) (e) (2, 0.36) (f) (20, 0.36)

FIG. 3. Phase diagrams for various parameters depicting the topological changes due to variation of μ while keeping z fixed. The parameters (μ, z) are mentioned in the subcaptions. Solid blue lines denote theoretical outcomes, whereas red circles denote Monte Carlo simulation results. The contours in the phase diagrams represent the variation of current and the value of current is depicted in the accompanying color bar.

qualitative changes take place, which are obtained as

$$\mu_{c_1} = \frac{1-z}{2-z}, \quad \mu_{c_2} = 0.5. \tag{27}$$

For $\mu \leqslant \mu_{c_1}$, the phase diagram exhibits only two stationary phases, L/L and L/S, whereas when $\mu_{c_1} < \mu \leqslant \mu_{c_2}$, another phase emerges, leading to three distinct phases, namely L/L, L/S, and S*/L. Moreover, for $\mu > \mu_{c_2}$, with the addition of five more regions (H/L, H/S*, H/H, S/H, and L/H), the phase schema now consists of eight phases. The schema remains asymmetric for $\mu < 1$ and becomes symmetric with respect to $\alpha = \beta$ line when $\mu = 1$. With further increase in μ, the system again loses its symmetry.

Additionally, it is observed that the region occupied by bulk-induced S*/L phase decreases with an increase in the number of particles in the system and finally vanishes as $\mu \to \infty$. However, the other bulk-induced shock phase, namely H/S*, persists in the limit $\mu \to \infty$. This is supported mathematically as the width of H/S* phase, $\Delta_{\mathrm{H/S^*}}$, is expressed as

$$\Delta_{\mathrm{H/S^*}} = \frac{\mu z(1-z)}{2-z} \tag{28}$$

and remains proportional to the filling factor.

It is observed from Table I that the densities of the defect-restricted phases remain unaffected by μ, implying the robustness of current in these phases with respect to μ. However, the same cannot be said about the remaining phases. Thus, it is expected that the current of the remaining phases is affected by the availability of particles: A dearth of particles reduces the entry rate, thus affecting the current. To demonstrate this, we have plotted Fig. 4 for $\alpha = 0.2$, $\beta = 25$, and $z = 0.36$, whereas μ is varied from 0 to 20 lying in L/L region, which displays monotonic increase in the current.

Now we move on to investigate the impact of defect on the stationary properties of the system.

B. Effect of defect dynamics

The defect kinetics is critical to comprehending the stationary state of the system. The transition rates of the particles are locally affected when the dynamic defect is incorporated at site m. However, when such kinetics are excluded, the dynamics are normal and uniform. We can assess the defect dynamics using our theoretical method and analyze its impact. It is interesting to note that while the defect kinetics of our model are controlled by three distinct parameters, namely k_+, k_-, and p_d, the theoretical method reveals much more simplified analysis where the impact of defect can be quantified by only one parameter: the obstruction factor z.

Figure 5 depicts the dependency of the stationary current in the H/L phase on obstruction factor z. As expected, the current decreases with an increase in the obstruction to the flow of particles.

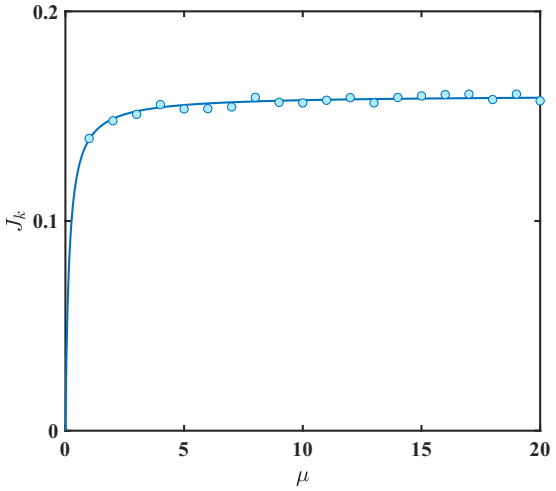

FIG. 4. Impact of filling factor μ on current: current J_k ($k \in \{1, 2\}$) increases with increment in μ. The other parameters are $\alpha = 0.2$, $\beta = 25$, and $z = 0.36$. Solid line represents theoretical outcome, whereas circles denote Monte Carlo simulation results.

For nonzero obstruction (i.e., $z \neq 0$), the defect-restricted phases appear in the phase diagrams which vanish at $z = 0$ as can be seen in Figs. 3(d) and 6, respectively. In the limiting case $z \to 0$, i.e., either $p_d \to 1$ or $\rho^* \to 0$, the defect is rendered ineffective and the current in H/L phase approaches the value 0.25, which agrees with the maximal current in the nondefective counterpart [36]. Moreover, the topology of the phase diagram thus derived is quite similarly to that of a homogeneous TASEP with reservoir crowding [36]. This is simply demonstrated by considering the following grouping of phases as listed below:

$$\text{L/L} \leftrightarrow \text{L}, \quad \text{M/M} \leftrightarrow \text{M}, \quad \text{H/H} \leftrightarrow \text{H}, \quad \text{L/S, S/H, L/H} \leftrightarrow \text{S}. \tag{29}$$

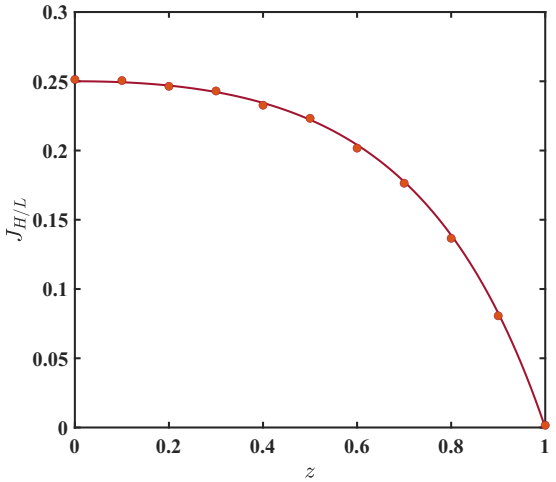

FIG. 5. Impact of obstruction factor z on current in the H/L phase (denoted as $J_{\text{H/L}}$). The parameter $z = 0$ (1) corresponds to minimum (maximum) obstruction to the flow of particles. The other parameter is $\mu = 1$. Solid line represents theoretical outcome, whereas circles denote Monte Carlo simulation results.

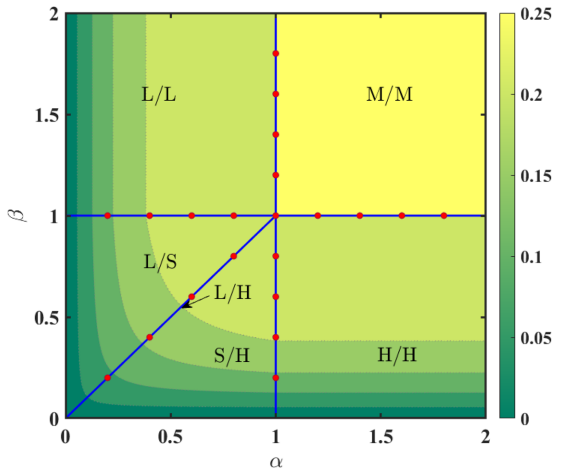

FIG. 6. Phase diagram for the parameters $\mu = 1$ and $z = 0$. Solid lines denote theoretical outcomes, whereas circles denote Monte Carlo simulation results. The contours and the color bar provide the visualization of current across the phases.

In another extreme case when $z = 1$, the particle flow is completely blocked leading to zero current in the system. In such a scenario, the phase diagram is completely occupied by H/L phase with the maximal sustainable current to be zero. This is supported mathematically by the expressions in Table I where the effective rates that govern the particle densities and currents become zero.

Now, we discuss the two categories of shock phases, bulk induced and boundary induced, in detail that arise in the phase diagram.

C. Shock dynamics

As discussed in previous sections, localized shock develops in the density profiles as a result of the system's finite number of particles. The phases admitting these shock can be categorized into two types: bulk induced and boundary induced. A bulk-induced shock has been seen to exist in the S*/L and H/S* phases. Meanwhile, a boundary-induced shock appears in L/S and S/H phases. In thermodynamic limit, the Eq. (9) becomes the common continuity equation, $\partial \rho_k / \partial t + \partial J_k / \partial x = 0$. The velocity of shock is then given by

$$V = \begin{cases} \bar{\beta} - \bar{\alpha}; & \text{for L/S and S/H phases,} \\ \beta_e - \alpha_e; & \text{for S*/L and H/S* phases.} \end{cases} \tag{30}$$

In order to obtain a shock in the bulk, the velocity of the shock must be zero [51,52]. Using this condition, the system in phases with shock are analyzed, whose details can be found in Appendix B.

Here we analyze the shock propagation on the lattice with respect to entry-exit rates in the α-β plane, whereas the other parameters remain fixed.

1. Bulk-induced shock

The system exhibits bulk-induced shocks as the lattice displays low-high-low density segments in the S*/L phase and high-low-high density segments in the H/S* phase. From the existence conditions provided in Table I, these phases vanish

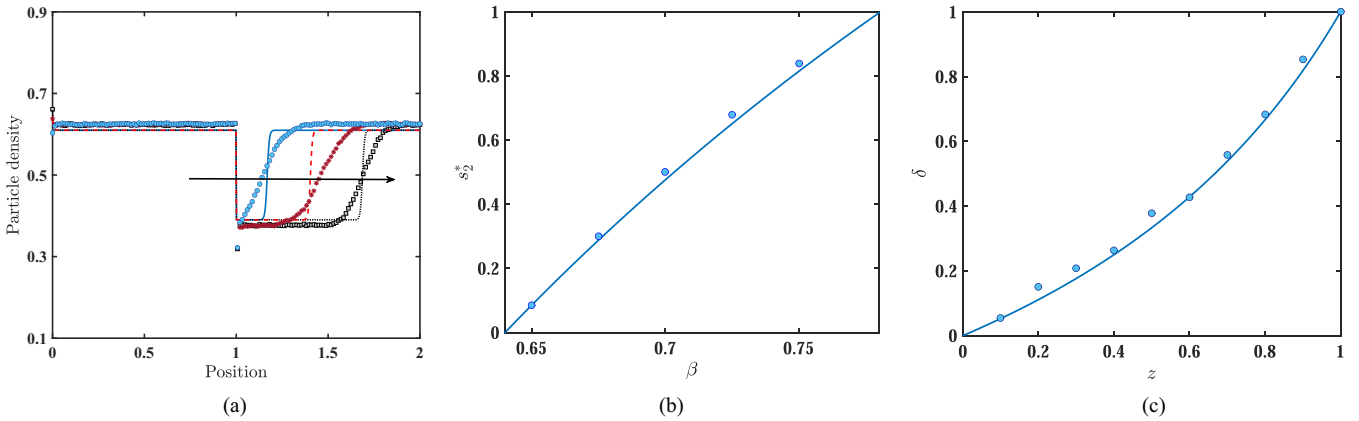

FIG. 7. (a) Movement of shock with respect to (a) β while α is fixed at 1.5. The shock position in density profiles move from right to left when β is increased from 0.66 to 0.72 at the difference of 0.3. (b) Variation of shock position s_2^* in the H/S* phase. (c) Change in shock height, δ, when β is varied. The other parameters are $\alpha = 1.5$, $\mu = 1$, and $z = 0.36$. Lines of various styles denote theoretical results, whereas the outcomes of Monte Carlo simulations are represented by symbols. The position from 0 (1) to 1 (2) denotes the sublattice L_1 (L_2).

as soon as the impact of defect wanes. Thus, the bulk-induced shocks emerge as a consequence of the defect dynamics. The position of shock in S*/L phase is given as

$$s_1^* = \frac{2\mu(1-z) + \alpha(2\mu-1)(2-z)}{\alpha z}, \tag{31}$$

whereas for the H/S* phase, the expression is

$$s_2^* = \frac{2[\beta - \mu(1-z)]}{\beta z}. \tag{32}$$

Their calculations are detailed in Appendix B. For finite system size, this shock is expressed as a tanh-type boundary layer, which was discussed in Sec. III. When $\alpha = 1.5$, the movement of shock with respect to increasing β is provided in Figs. 7(a) and 7(b). Owing to the fact that the properties of the bulk-induced phases are independent of the entry-exit rates, the shock height remains constant throughout each of these phases. The height of this shock increases with respect to the obstruction to the flow of particles, which can be seen in Fig. 7(c). It is observed that in absence of any obstruction, the shock height becomes zero, which asserts that this phase vanishes when defect is ineffective.

2. *Boundary induced shock*

The boundary-induced shocks appear in S/H and L/S phases and their positions are given by

$$s_1 = \frac{2[\beta - \alpha(-1+\beta+\mu)]}{\alpha(1-2\beta)+\beta} \tag{33}$$

and

$$s_2 = \frac{\alpha(1-2\mu)+\beta}{\alpha(1-2\beta)+\beta}, \tag{34}$$

respectively. The detailed calculations are provided in Appendix B. These shocks appear as a rapidly changing solution for finite systems and are given by tanh-type solutions as discussed in Sec. III. It is observed that the shock emerges from the right boundary of the lattice and moves toward the left with respect to α. To visualize the shock propagation, we have plotted in Fig. 8(a) density profiles for different α while keeping the other parameters fixed. Analogously, the shock position shifts from left to right with respect to β, as can be seen in Fig. 8(b). Moreover, the shock height in these phases decrease monotonically with respect to α, which is demonstrated in Fig. 8(c). The parameters μ and z are fixed at 1 and 0.36, respectively. Due to the symmetry of phase diagram at $\mu = 1$, the shock height with respect to β for fixed α coincides with Fig. 8(c).

On contrary to the bulk-induced shock phases, the stationary properties of these phases remain unaffected by the defect kinetics, which can be observed from the expressions provided in the Table I. It can also be seen from Eqs. (33) and (34) that the position of shock remains independent of the defect dynamics.

To summarize, it is seen by theoretical analysis that our system exhibits nine stationary phases with at most eight phases appearing in a phase diagram for given dynamics. Some of these phases include shock which may either be bulk-induced or boundary-induced, and the position of shock and their height are obtained analytically. The critical points enabling the qualitative changes in phase schema are obtained. All the theoretical arguments have been backed intuitively and validated via Monte Carlo simulations.

VI. CONCLUSION

In this study, a theoretical model is developed to investigate the kinetics of a system having a constraint on the number of particles in the presence of a dynamic defect that may slow down particle flux. Further, reservoir crowding also features in the system which regulates both entry and exit of particles as functions of number of particles in the reservoir. We generalized a totally asymmetric simple exclusion process exhibiting reservoir crowding by incorporating the effect of reversible defect on a special site. The model is analyzed theoretically using a simple mean-field approach to understand the stationary properties of the system. The defect site causes inhomogeneity on the lattice, and we divided our system into two connected sublattices. This allows us to characterize the dynamics of the particles at each homogeneous

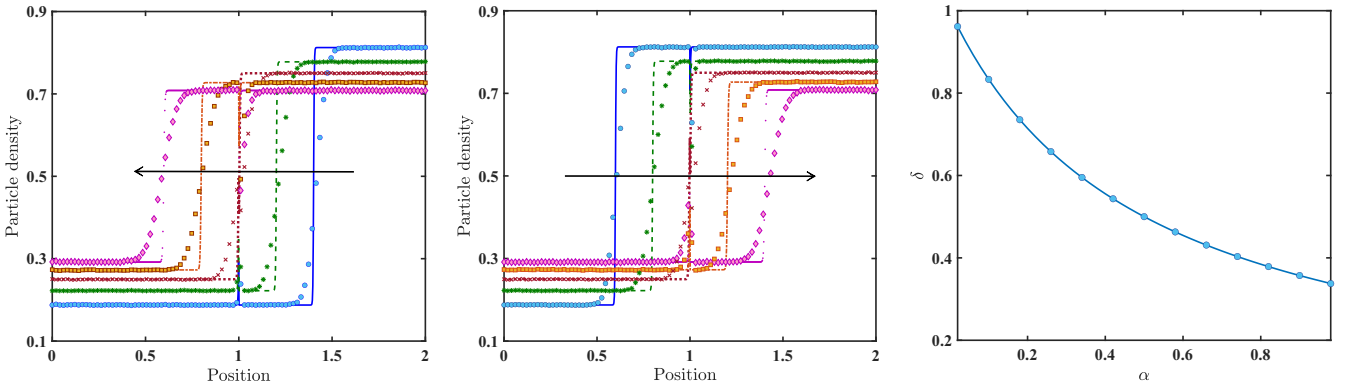

FIG. 8. Movement of shock with respect to (a) α while β is fixed at 0.5 and (b) β while α is fixed at 0.5. The shock position in density profiles move from right to left (left to right) when α (β) is increased from 0.3 to 0.7 at the difference of 0.1. (c) Change in shock height, δ, when $\beta = 0.5$ and α is varied. The other parameters are $\mu = 1$ and $z = 0.36$. Lines of various styles denote theoretical results, whereas the outcomes of Monte Carlo simulations are represented by symbols. The position from 0 (1) to 1 (2) denotes the sublattice L_1 (L_2).

sublattice individually. The boundary-layer analysis to provide the complete density profile for a finite system has also been discussed.

A salient feature of our theoretical approach is the reduction of parameter space corresponding to the defect dynamics from three to one. The parameters quantifying the binding and unbinding of dynamic defect as well as the slowdown rate which collectively describe the defect kinetics in the model have been replaced by another parameter z, termed the obstruction factor. Interestingly, it does not restrict the degree of freedom of the defect dynamics and significantly simplifies the mathematical analysis.

Utilizing the theoretical approach, of 16 probable phases, we discarded six phases based on physical arguments and one phase based on analytical arguments. We established that there are at most nine potential stationary phases displayed by the system based on the kinetics. The properties of five phases among these are regulated by processes at the entry or exit from the lattice, and so are not affected by defect dynamics in a major way. However, the remaining phases are heavily dependent on the obstruction provided by the defect. Further, the proposed model exhibits two types of shocks: bulk induced and boundary induced. The former vanishes as the effect of defect fades. The propagation of shock and their height have been investigated theoretically.

The composition of the phase diagram is found to be strongly dependent on the population of the system which is characterized by filling factor. On varying the filling factor, the phase diagram is found to undergo qualitative changes at two critical values which have been obtained analytically. It is found that the defect gives rise to defect-restricted phases and does not impact the properties of the remaining phases. Our theoretical predictions match with Monte Carlo simulation findings, indicating that our theoretical technique reflects the process's mechanics efficiently. Although the theoretical approach and Monte Carlo simulations have been provided for a specific pair of functions, our method also works for different choices of functions that fits certain conditions reflecting the real processes.

The primary purpose of our proposed work was to explain the dynamic properties of the system in study, and the conclusions given were able to characterize the effect of dynamic defects. We have considered a generic model that can be implemented to comprehend the behavior of various transport processes, both natural and human-made. In the future, one may include several other dynamics such as interactions among particles, Langmuir kinetics, etc., to study a more generalized version.

ACKNOWLEDGMENT

A.K.G. acknowledges support from DST-SERB, Government of India (Grants No. CRG/2019/004669 and No. MTR/2019/000312).

APPENDIX A: NUMERICAL METHOD FOR DENSITY PROFILES OF PARTICLES

Here we provide an alternative method for obtaining density profiles using numerical techniques for the following reasons. First, the procedure is less sophisticated than the analytical approach mentioned in Secs. III and IV. Moreover, similarly to the aforementioned approach, this method also provides the complete solution to the finite system. Second, unlike the theoretical approach, this method can be readily modified according to a more generalized model by incorporating the changes in master equation. Finally, this method can be employed to obtain the solution where the choice of functions for Eq. (3) leads to an analytically intractable form.

We begin by discretizing the partial differential equation in Eq. (9) using a finite difference scheme where time and space derivatives are replaced using forward and central difference formulas, respectively. Taking $\Delta x = 1/L$ and an appropriate Δt that satisfies the stability condition $\Delta t/\Delta x^2 \leqslant 1$, the solution is obtained in the limit $n \to \infty$ where n is the number of time steps for $1 < i < L$ to ensure the occurrence of steady

state. The discretized equation is given as

$$\rho_{i,k}^{n+1} = \rho_{i,k}^{n} + \frac{\epsilon}{2}\frac{\Delta t}{\Delta x^2}\left(\rho_{i+1,k}^{n} - 2\rho_{i,k}^{n} + \rho_{i-1,k}^{n}\right) + \frac{\Delta t}{2\Delta x}\left(2\rho_{i,k}^{n} - 1\right)\left(\rho_{i+1,k}^{n} - \rho_{i-1,k}^{n}\right), \tag{A1}$$

where $k \in \{1, 2\}$ and $\rho_{i,k}^{n}$ is the mean-field density of the site i in sublattice L_k at time step n. Due to the definition of the proposed model, both sublattices interact with each other at their boundaries. Hence, the boundary conditions are implemented by using the discrete equations with statistical average replaced by the mean-field density and are obtained as

$$\begin{aligned}
\rho_{1,1}^{n+1} &= \rho_{1,1}^{n} + \Delta t\alpha\left[1 - \frac{\sum_{i=1}^{L}(\rho_{i,1} + \rho_{i,2})}{N_{\text{tot}}}\right]\left(1 - \rho_{1,1}^{n}\right) \\
&\quad - \Delta t\,\rho_{1,1}^{n}\left(1 - \rho_{2,1}^{n}\right), \\
\rho_{L,1}^{n+1} &= \rho_{L,1}^{n} + \Delta t\left[\rho_{L-1,1}^{n}\left(1 - \rho_{L,1}^{n}\right) - p_d\rho^{*}\rho_{L,1}^{n}\left(1 - \rho_{1,2}^{n}\right)\right. \\
&\quad \left. - (1 - \rho^{*})\rho_{L,1}^{n}\left(1 - \rho_{1,2}^{n}\right)\right], \\
\rho_{1,2}^{n+1} &= \rho_{1,2}^{n} + \Delta t\left[p_d\rho^{*}\rho_{L,1}^{n}\left(1 - \rho_{1,2}^{n}\right) - \rho_{1,2}^{n}\left(1 - \rho_{2,2}^{n}\right)\right. \\
&\quad \left. + (1 - \rho^{*})\rho_{L,1}^{n}\left(1 - \rho_{1,2}^{n}\right)\right], \\
\rho_{L,2}^{n+1} &= \rho_{L,2}^{n} + \Delta t\,\rho_{L-1,2}^{n}\left(1 - \rho_{L,2}^{n}\right) \\
&\quad - \Delta t\beta\left[1 - \frac{\sum_{i=1}^{L}(\rho_{i,1} + \rho_{i,2})}{N_{\text{tot}}}\right]\rho_{L,2}^{n}.
\end{aligned} \tag{A2}$$

The density of defect also evolves with time, and therefore ρ^{*} must be determined using the discrete equation at each time step. This equation is expressed as

$$\rho^{*n+1} = \rho^{*n} + \Delta t[(1 - \rho^{*n})k_{+} - \rho^{*n}k_{-}]. \tag{A3}$$

Equation (A1), together with Eqs. (A2) and (A3), provides the density profiles for both the sublattices as well as the defect density. Even though this method is straightforward, one must note that this method does not provide any further analysis explicitly, which obstructs the extensive study of proposed model. Further, this method requires all three parameters, k_{+}, k_{-}, and p_d, to be studied individually, even though they are revealed to be related using our theoretical analysis.

APPENDIX B: FEASIBLE/INFEASIBLE PHASES

In this section, we delineate the methodology to obtain the altered rates and the position of shock, wherever applicable, for the probable phases.

(1) L/L: In this case, the particles display low-density phase in both sublattices and their densities are given by $\rho_1 = \bar{\alpha}$ and $\rho_2 = \alpha_e$. Using the continuity of current, these densities must be equal i.e., $\alpha_e = \bar{\alpha} = \alpha r/\mu$. Further, employing $\rho_2(0) = \alpha_e$ in Eq. (19) gives $\beta_e = (1 - \alpha_e)(1 - z)$. Finally, by using PNC, the quotient of the reservoir is calculated as

$$r = \frac{\mu^2}{\alpha + \mu}, \tag{B1}$$

which is used to evaluate the altered rates.

(2) H/H: Utilizing the methodology similar to that of the L/L phase, the quotient of the reservoir is obtained as

$$r = \frac{\mu(-1 + \beta + \mu)}{\beta + \mu}, \tag{B2}$$

and subsequently the altered rates can be obtained.

(3) L/S: This case occurs when sublattices L_1 and L_2 display a low-density phase and shock phase, respectively. Thus, the particle densities are given as $\rho_1 = \bar{\alpha}$ and

$$\rho_2 = \begin{cases} \alpha_e; & 0.5 \leqslant x \leqslant s_2, \\ 1 - \bar{\beta}; & s_2 < x \leqslant 1, \end{cases} \tag{B3}$$

where s_2 gives the position of shock in sublattice L_2. By continuity of current, we have $\alpha_e = \bar{\alpha}$, and due to the coupling of current, $\beta_e = (1 - \alpha_e)(1 - z)$. Moreover, for the existence of shock, the condition $\alpha_e = \bar{\beta}$ must hold, which gives

$$r = \frac{\beta\mu}{\alpha + \beta}. \tag{B4}$$

Finally, by using PNC, the position of shock is

$$s_2 = \frac{\alpha(1 - 2\mu) + \beta}{\alpha(1 - 2\beta) + \beta}. \tag{B5}$$

(4) S/H: By arguments similar to those for the L/S phase, the quotient of the reservoir is obtained as

$$r = \frac{\beta\mu}{\alpha + \beta}, \tag{B6}$$

and the position of shock in sublattice L_1 is expressed as

$$s_1 = \frac{2[\beta - \alpha(-1 + \beta + \mu)]}{\alpha(1 - 2\beta) + \beta}. \tag{B7}$$

(5) H/L: This case results in particles displaying high-density and low-density phases in sublattices L_1 and L_2, respectively. Thus, the particle densities are expressed as $\rho_1 = 1 - \beta_e$ and $\rho_2 = \alpha_e$. By deploying the coupling of current, the effective rates are given as

$$\alpha_e = \beta_e = \frac{1 - z}{2 - z}. \tag{B8}$$

Subsequently, using PNC yields the following value for quotient of reservoir:

$$r = \mu - \frac{1}{2}. \tag{B9}$$

Clearly, as $z \to 1$, the particle densities in both sublattices tend to 0.5 and the condition of existence of this phase is violated. Moreover, in such a limiting case, i.e., when the defect dynamics have no effect on the system, it transitions to the M/M phase.

(6) S*/L: This scenario occurs when the sublattices L_1 and L_2 display a shock phase and a low-density phase, respectively. Thus, the particle densities are expressed as

$$\rho_1 = \begin{cases} \bar{\alpha}; & 0 \leqslant x \leqslant s_1^{*}, \\ 1 - \beta_e; & s_1^{*} < x \leqslant 1, \end{cases} \tag{B10}$$

and $\rho_2 = \alpha_e$. On using the current coupling, the following expression for the effective rates is obtained:

$$\alpha_e = \beta_e = \frac{1 - z}{2 - z}. \tag{B11}$$

For existence of shock, the condition $\beta_e = \bar{\alpha}$ must be satisfied, resulting in the reservoir quotient to be expressed as

$$r = \frac{\mu}{\alpha}\left(\frac{1-z}{2-z}\right). \tag{B12}$$

By employing PNC, the position of shock is obtained as

$$s_1^* = \frac{2\mu(1-z)+\alpha(2\mu-1)(2-z)}{\alpha z}. \tag{B13}$$

(7) H/S*: By utilizing the reasoning analogous to that for S*/L, the quotient of the reservoir is evaluated as

$$r = \frac{\mu[-1+z+\beta(2+z)]}{\beta(2+z)}, \tag{B14}$$

and the position of shock in sublattice L_2 is given by

$$s_2^* = \frac{2[\beta-\mu(1-z)]}{\beta z}. \tag{B15}$$

(8) L/H: When the particles are in the low-density phase and high-density phases in sublattices L_1 and L_2, respectively, their densities are given by $\rho_1 = \bar{\alpha}$ and $\rho_2 = 1-\bar{\beta}$. Due to the coupling of current, the reservoir quotient is evaluated as

$$r = \frac{\mu(-1+\beta+2\mu)}{\alpha+\beta+2\mu}, \tag{B16}$$

whereas the continuity of current yields

$$r = \frac{\beta\mu}{\alpha+\beta}. \tag{B17}$$

The reservoir must hold a unique value, and therefore expressions provided by Eqs. (B16) and (B17) must be equal, which gives the existence curve of this phase as

$$\alpha = \frac{\beta}{2\mu-1}. \tag{B18}$$

This phase arises on the transition line between L/S and S/H.

(9) M/M: In this phase, both sublattices exhibit maximal current and their densities are equal to 0.5. Therefore, the reservoir holds the remaining particles and its quotient is given by

$$r = \mu - \tfrac{1}{2}. \tag{B19}$$

Subsequently, the altered rates are obtained and it is observed that this phase exists only in the case when defect is ineffective, i.e., $z = 0$.

Theoretically discarded phase

The S/S phase arises when both sublattices display shock phase. On obtaining the altered rate and existence conditions, this phase is found to be on the phase transition curve between S*/L and L/S as well as H/S* and S/H. This means the position of shock is only on the boundaries in these sublattices. Thus this phase can be discarded.

[1] A. Schadschneider, D. Chowdhury, and K. Nishinari, *Stochastic Transport in Complex Systems: From Molecules to Vehicles* (Elsevier, Amsterdam, 2010).

[2] T. Chou, K. Mallick, and R. K. Zia, Non-equilibrium statistical mechanics: From a paradigmatic model to biological transport, Rep. Prog. Phys. **74**, 116601 (2011).

[3] D. Chowdhury, L. Santen, and A. Schadschneider, Statistical physics of vehicular traffic and some related systems, Phys. Rep. **329**, 199 (2000).

[4] X. Shi, Z. Ye, N. Shiwakoti, and Z. Li, A review of experimentalstudies on complex pedestrian movement behaviors, in *Proceedings of the 15th COTA International Conference of Transport* (American Society of Civil Engineers, Beijing, China, 2015), pp. 1081–1096.

[5] T. Kretz, A. Grünebohm, and M. Schreckenberg, Experimental study of pedestrian flow through a bottleneck, J. Stat. Mech. (2006) P10014.

[6] M. Schliwa and G. Woehlke, Molecular motors, Nature (Lond.) **422**, 759 (2003).

[7] F. Jülicher, A. Ajdari, and J. Prost, Modeling molecular motors, Rev. Mod. Phys. **69**, 1269 (1997).

[8] B. Derrida, An exactly soluble non-equilibrium system: The asymmetric simple exclusion process, Phys. Rep. **301**, 65 (1998).

[9] G. M. Schütz, Critical phenomena and universal dynamics in one-dimensional driven diffusive systems with two species of particles, J. Phys. A: Math. Gen. **36**, R339 (2003).

[10] B. Derrida, Non-equilibrium steady states: Fluctuations and large deviations of the density and of the current, J. Stat. Mech. (2007) P07023.

[11] R. A. Blythe and M. R. Evans, Nonequilibrium steady states of matrix-product form: A solver's guide, J. Phys. A: Math. Theor. **40**, R333 (2007).

[12] J. Krug, Phase separation in disordered exclusion models, Braz. J. Phys. **30**, 97 (2000).

[13] V. Popkov, L. Santen, A. Schadschneider, and G. M. Schütz, Empirical evidence for a boundary-induced nonequilibrium phase transition, J. Phys. A: Math. Gen. **34**, L45 (2001).

[14] K. Nagel and M. Schreckenberg, A cellular automaton model for freeway traffic, J. Phys. I France **2**, 2221 (1992).

[15] C. T. MacDonald and J. H. Gibbs, Concerning the kinetics of polypeptide synthesis on polyribosomes, Biopolymers **7**, 707 (1969).

[16] D. Chowdhury, Resource letter PBM-1: Physics of biomolecular machines, Am. J. Phys. **77**, 583 (2009).

[17] T. Tripathi and D. Chowdhury, Interacting rna polymerase motors on a dna track: Effects of traffic congestion and intrinsic noise on RNA synthesis, Phys. Rev. E **77**, 011921 (2008).

[18] S. Klumpp and T. Hwa, Stochasticity and traffic jams in the transcription of ribosomal RNA: Intriguing role of termination and antitermination, Proc. Natl. Acad. Sci. USA **105**, 18159 (2008).

[19] M. Sahoo and S. Klumpp, Transcriptional proofreading in dense RNA polymerase traffic, Europhys. Lett. **96**, 60004 (2011).

[20] C. T. MacDonald, J. H. Gibbs, and A. C. Pipkin, Kinetics of biopolymerization on nucleic acid templates, Biopolymers **6**, 1 (1968).
[21] L. B. Shaw, R. K. P. Zia, and K. H. Lee, Totally asymmetric exclusion process with extended objects: A model for protein synthesis, Phys. Rev. E **68**, 021910 (2003).
[22] B. Derrida and J. L. Lebowitz, Exact large deviation function in the asymmetric exclusion process, Phys. Rev. Lett. **80**, 209 (1998).
[23] J. de Gier and F. H. L. Essler, Bethe Ansatz Solution of the Asymmetric Exclusion Process with Open Boundaries, Phys. Rev. Lett. **95**, 240601 (2005).
[24] A. Parmeggiani, T. Franosch, and E. Frey, Phase Coexistence in Driven One-Dimensional Transport, Phys. Rev. Lett. **90**, 086601 (2003).
[25] S. Klumpp and R. Lipowsky, Active Diffusion of Motor Particles, Phys. Rev. Lett. **95**, 268102 (2005).
[26] B. Waclaw, J. Cholewa-Waclaw, and P. Greulich, Totally asymmetric exclusion process with site-wise dynamic disorder, J. Phys. A: Math. Theor. **52**, 065002 (2019).
[27] A. B. Kolomeisky, Asymmetric simple exclusion model with local inhomogeneity, J. Phys. A: Math. Gen. **31**, 1153 (1998).
[28] S. Mukherji, Asymmetric simple exclusion process with position-dependent hopping rates: Phase diagram from boundary-layer analysis, Phys. Rev. E **97**, 032130 (2018).
[29] A. K. Gupta and I. Dhiman, Asymmetric coupling in two-lane simple exclusion processes with langmuir kinetics: Phase diagrams and boundary layers, Phys. Rev. E **89**, 022131 (2014).
[30] P. Greulich, L. Ciandrini, R. J. Allen, and M. C. Romano, Mixed population of competing totally asymmetric simple exclusion processes with a shared reservoir of particles, Phys. Rev. E **85**, 011142 (2012).
[31] L. J. Cook and R. Zia, Feedback and fluctuations in a totally asymmetric simple exclusion process with finite resources, J. Stat. Mech. (2009) P02012.
[32] L. J. Cook, J. J. Dong, and A. LaFleur, Interplay between finite resources and a local defect in an asymmetric simple exclusion process, Phys. Rev. E **88**, 042127 (2013).
[33] C. A. Brackley, L. Ciandrini, and M. C. Romano, Multiple phase transitions in a system of exclusion processes with limited reservoirs of particles and fuel carriers, J. Stat. Mech. (2012) P03002.
[34] D. Adams, B. Schmittmann, and R. Zia, Far-from-equilibrium transport with constrained resources, J. Stat. Mech. (2008) P06009.
[35] L. J. Cook, R. K. P. Zia, and B. Schmittmann, Competition between multiple totally asymmetric simple exclusion processes for a finite pool of resources, Phys. Rev. E **80**, 031142 (2009).
[36] A. Haldar, P. Roy, and A. Basu, Asymmetric exclusion processes with fixed resources: Reservoir crowding and steady states, Phys. Rev. E **104**, 034106 (2021).
[37] B. Pal and A. K. Gupta, Persistence of spontaneous symmetry breaking in bidirectional transport system with reservoir crowding, J. Phys. A: Math. Theor. **54**, 405002 (2021).
[38] J. Elf, G.-W. Li, and X. S. Xie, Probing transcription factor dynamics at the single-molecule level in a living cell, Science **316**, 1191 (2007).
[39] S.-K. Choi and M. H. Saier Jr, Regulation of sigl expression by the catabolite control protein ccpa involves a roadblock mechanism in bacillus subtilis: Potential connection between carbon and nitrogen metabolism, J. Bacteriol. **187**, 6856 (2005).
[40] P. Pierobon, M. Mobilia, R. Kouyos, and E. Frey, Bottleneck-induced transitions in a minimal model for intracellular transport, Phys. Rev. E **74**, 031906 (2006).
[41] L. B. Shaw, A. B. Kolomeisky, and K. H. Lee, Local inhomogeneity in asymmetric simple exclusion processes with extended objects, J. Phys. A: Math. Gen. **37**, 2105 (2004).
[42] K. Qiu, X. Yang, W. Zhang, D. Sun, and Y. Zhao, Density profiles in the totally asymmetric exclusion processes with both local inhomogeneity and langmuir kinetics, Physica A **373**, 1 (2007).
[43] M. Sahoo and S. Klumpp, Asymmetric exclusion process with a dynamic roadblock and open boundaries, J. Phys. A: Math. Theor. **49**, 315001 (2016).
[44] M. Sahoo, J. Dong, and S. Klumpp, Dynamic blockage in an exclusion process, J. Phys. A: Math. Theor. **48**, 015007 (2015).
[45] A. Jindal, A. B. Kolomeisky, and A. K. Gupta, The role of dynamic defects in transport of interacting molecular motors, J. Stat. Mech. (2020) 043206.
[46] F. Turci, A. Parmeggiani, E. Pitard, M. C. Romano, and L. Ciandrini, Transport on a lattice with dynamical defects, Phys. Rev. E **87**, 012705 (2013).
[47] C. Appert-Rolland, M. Ebbinghaus, and L. Santen, Intracellular transport driven by cytoskeletal motors: General mechanisms and defects, Phys. Rep. **593**, 1 (2015).
[48] C. Janke and M. Kneussel, Tubulin post-translational modifications: Encoding functions on the neuronal microtubule cytoskeleton, Trends Neurosci. **33**, 362 (2010).
[49] G. Schötz and E. Domany, Phase transitions in an exactly soluble one-dimensional exclusion process, J. Stat. Phys. **72**, 277 (1993).
[50] B. Derrida, E. Domany, and D. Mukamel, An exact solution of a one-dimensional asymmetric exclusion model with open boundaries, J. Stat. Phys. **69**, 667 (1992).
[51] A. B. Kolomeisky, G. M. Schütz, E. B. Kolomeisky, and J. P. Straley, Phase diagram of one-dimensional driven lattice gases with open boundaries, J. Phys. A: Math. Gen. **31**, 6911 (1998).
[52] L. Santen and C. Appert, The asymmetric exclusion process revisited: Fluctuations and dynamics in the domain wall picture, J. Stat. Phys. **106**, 187 (2002).